

# Exoskeletal strength and cuticle composite profile of the acorn weevil rostrum

M. Andrew Jansen,<sup>1,\*</sup> Jason Williams,<sup>2</sup> Nikhilesh Chawla,<sup>2</sup> and Nico M. Franz<sup>1</sup>

<sup>1</sup>School of Life Sciences, Arizona State University, Tempe, AZ 85287, USA

<sup>2</sup>School for Engineering of Matter, Energy, and Transport,  
Arizona State University, Tempe, AZ 85287, USA

(Dated: March 15, 2019)

The acorn weevil (*Curculio* Linnaeus, 1758) rostrum (snout) exhibits remarkable flexibility and toughness derived from the microarchitecture of its exoskeleton. Here we characterize modifications to the composite profile of the rostral cuticle that simultaneously enhance the flexibility and fracture toughness of the distal portion of the snout. Using Classical Lamine Plate Theory, we estimate the effect of these modifications on the elastic behavior of the exoskeleton. We show that the tensile behavior of the rostrum across six *Curculio* species with high morphological variation correlates with changes in the relative layer thicknesses and orientation angles of layers in the exoskeleton. Accordingly, increased endocuticle thickness is strongly correlated with increased tensile strength. Rostrum stiffness is shown to be inversely correlated with fracture toughness; thus allowing a highly curved rostrum to completely straighten without structural damage. Finally, we identify exocuticle rich invaginations of the occipital sutures both as a likely site of crack initiation in tensile failure, and as a source of morphological constraint on the evolution of the rostrum in *Curculio* weevils.

The exoskeleton of Coleoptera (beetles) is a hierarchically structured, fibrous composite – characterized by variously arranged  $\alpha$ -chitin (N-acetylglucosamine) nanofibrils that are embedded in a heterogeneous protein matrix [1–3]. Although  $\alpha$ -chitin is brittle and strongly anisotropic, beetle cuticle is simultaneously rigid and tough due to its unique laminate microstructure (reviewed in [4–6]), characterized in detail below. Impact-prone areas and exaggerated structures in arthropods generally exhibit cuticle organization that resists deformation and fracture [7–11]. However, acorn weevils in the genus *Curculio* Linnaeus, 1758<sup>1</sup> (Curculionidae in the sense of [13]) instead exhibit unusual distal flexibility in an elongate extension of the head called the rostrum (snout) [1, 14–16]. The rostrum is a hollow, strongly curved (over 90° in some species), cylindrical, exoskeletal extension of the otherwise nearly-spherical head, which bears at its apex the terminal chewing mouthparts [16–20]. This structure is used by the female to feed on fruit (plant) tissue and to excavate sites for egg-laying (oviposition, see Fig. 1). The rostrum can be repeatedly bent, without evident damage, and despite being composed of the same material as other rigid body parts [1, 14–16]. By maintaining constant pressure on the snout and rotating around the bore-hole, females are able to flex the rostrum into a straightened configuration and produce a linear channel into the fruit. A single adult female may prepare hundreds of such sites [15, 21, 22].

Despite its documented performance in many *Curculio*

species [15, 16, 21, 22], it remains unknown how the rostrum of female acorn weevils can withstand the repeated, often extreme bending incurred during the process of egg-chamber excavation. In this study, we therefore characterize the composite profile of the rostral cuticle to account for the observed flexibility of the snout. We show that the relative layer thicknesses and fiber orientation angles of the exocuticle and endocuticle of the rostrum are strongly differentiated from the head capsule and other body parts. The effect of these differences on the elasticity of the cuticle is estimated using Classical Laminate Plate Theory (CLPT). Recent studies have shown that the yield strength of the beetle exoskeleton is lower in tension than compression [23]. To assess the validity of these findings, we compare the ultimate tensile strength of the rostrum across species and snout morphotypes. We also report displacement-controlled load cycling results for the snout of one *Curculio* species with strongly curved morphology. Our results indicate that an increase in the volume fraction of endocuticle in the rostrum conveys higher tensile strength at the rostral apex across all tested species; and further, that a strongly curved rostrum can be flexed repeatedly without harm to the structure.

[NMF note: Feel that intro could be shortened by not "giving away" so many results. Maybe 3-5 phrases less in 2 final paragraphs of intro]

We additionally describe the fracture mechanics of the snout, while considering how modification of the cuticle may prevent crack formation during oviposition. [Based on our findings, we posit that the composite profile of the rostral apex enables the snout to undergo repeated distal flexion while remaining within the elastic limits of the material, mitigating the risk of structural damage, and without evident alteration of the mechanical properties of the individual components of the cuticle across the structure and between species.] Accordingly, the flexibility and tensile strength of the rostrum appear to be

\* corresponding author, email: majanse1@asu.edu

<sup>1</sup> Pursuant to the International Code of Zoological Nomenclature, the first mention of any specific epithet will include the full genus and species names as a binomen (two-part name) followed by the author and date of publication of the name. This is not an in-line reference; it is a part of the name itself and refers to a particular act establishing the validity and fixing the identity of the corresponding name by that author [12].

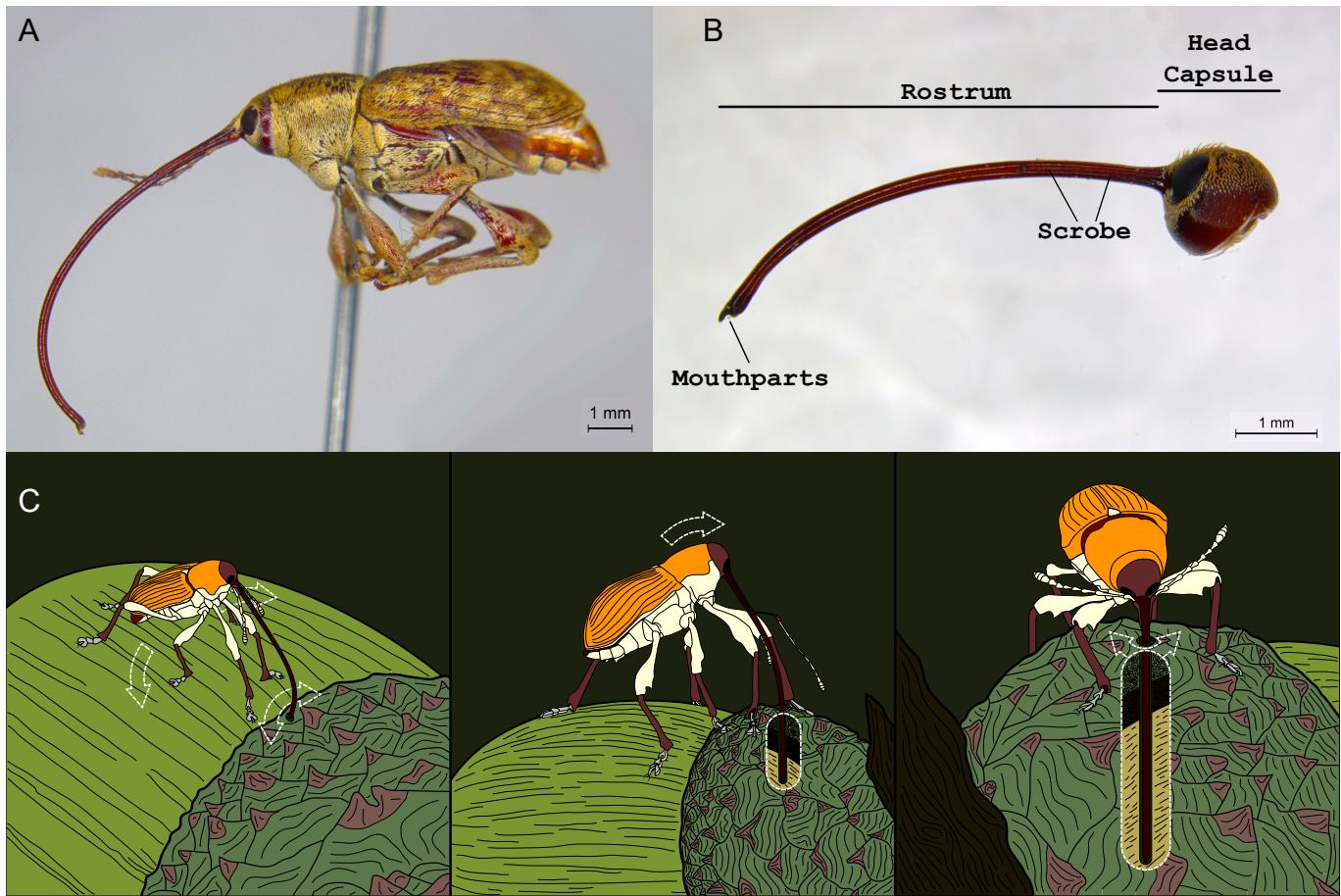


**FIG. 1. Morphology and oviposition behavior of female *Curculio* weevils.** **a**, Lateral habitus image of female *Curculio sayi* (Gyllenhal, 1836) featuring the elongate, strongly curved rostrum. **b**, Lateral view of the head of a female specimen of *Curculio longinasus* Chittenden, 1927, with major anatomical features indicated. **c**, Illustration of the oviposition behavior, proceeding from left to right: a female makes an incision in the host fruit, flexes the head directly over the bore hole using the front legs, then maintains tension on the snout while rotating to excavate a linear channel into the fruit. During this process, the female rostrum is bent until completely straight.

74 derived exclusively from modification of the composite  
75 architecture of the exoskeleton. This is the first time  
76 that a modified composite profile has been reported as  
77 a means of enhancing structural elasticity in the insect  
78 exoskeleton (though see [24]).

## 79 I. MICROSTRUCTURE OF THE CURCULIO 80 ROSTRUM

81 In arthropods – including beetles – the exocuticle is  
82 comprised of numerous unidirectional laminae of chitin  
83 nanofibrils. Each layer is the thickness of a single fiber  
84 (2–4 nm) embedded in a proteinaceous matrix [25, 26].  
85 These layers are stacked at a more or less constant an-  
86 gle to each other, forming a quasi-isotropic laminate  
87 known as the Bouligand structure [6, 27, 28]. This lay-  
88 out effectively mitigates the strong anisotropy of  $\alpha$ -chitin,  
89 thus yielding a versatile building material for the ex-  
90 oskeleton [2, 25, 26, 29]. Beetle endocuticle, however,

91 is unique among arthropods and is comprised of large  
92 – 1–5  $\mu\text{m}$  diameter in *Curculio* – unidirectional bun-  
93 dles of chitin, called macrofibers. Chitin macrofibers  
94 are orthotropic (axial:  $E_1 = 8.5 \text{ GPa}$ ; transverse:  
95  $E_2 = E_3 = 0.52 \text{ GPa}$  [1]), and arranged in uni-  
96 directional plies, as depicted in Figs. 2, 3 [4, 5]. Typi-  
97 cally, adjacent macrofiber laminae are paired and pseudo-  
98 orthogonal – i.e., angled nearly 90° to each other (see  
99 Fig. 3; [30]) – with a constant stacking angle between  
100 pairs, although other configurations have been observed  
101 [3–5, 31]. This geometric sequence of the macrofiber lam-  
102 inae yields an approximately transversely isotropic com-  
103 posite, similar to the Bouligand structure [5, 26]. No-  
104 tably, the resulting laminate is less rigid than the exocu-  
105 ticle, but exhibits greater toughness because the pseudo-  
106 orthogonal plies effectively inhibit crack formation and  
107 propagation between successive layers [3–5].

108 Serial thin sectioning and scanning electron microscopy  
109 of fractured *Curculio* specimens reveals that endocuti-  
110 cle in the head capsule fits this general profile, with an

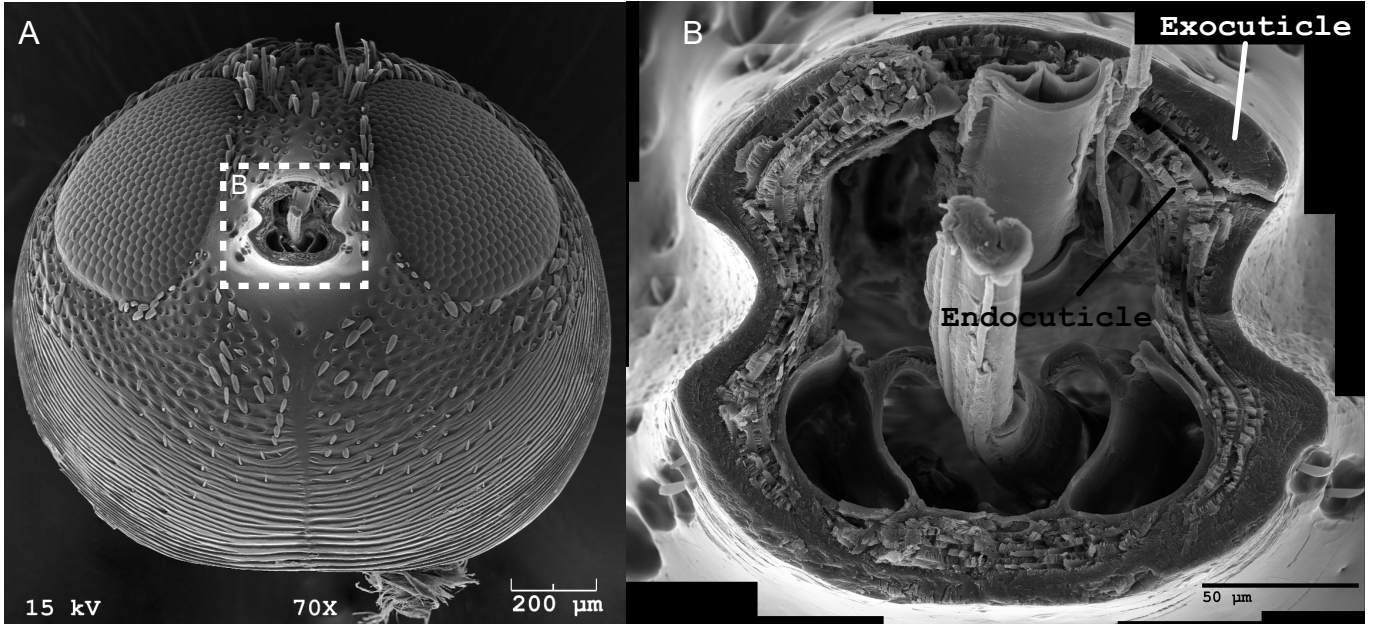


**FIG. 2. Gross divisions of cuticle in the female *Curculio* rostrum.** **a**, Scanning electron micrograph of the head capsule, in frontal view, of female *Curculio sulcatus* (Casey, 1897), with the rostrum removed. **b**, Magnified view of the junction between the rostrum and head capsule, showing the division of the cuticle into two general regions: the exocuticle and the endocuticle.

angle of nearly  $30^\circ$  between successive pairs of pseudo-orthogonal plies. Additionally, in the head capsule, the thickness of the exocuticle and endocuticle in cross-section is nearly equal – typically between 20–30  $\mu\text{m}$ . However, the cuticle composite lay-up of the rostral apex is strongly differentiated from the head capsule, as shown in Fig. 3. Distally the exocuticle is reduced to a thin shell (ca. 5  $\mu\text{m}$ ), with the endocuticle thickened to offset this reduction and maintain a constant cuticle thickness (ca. 50  $\mu\text{m}$  total) throughout its length. Moreover, the endocuticular macrofibers exhibit no rotation between successive pseudo-orthogonal plies; and are oriented at approximately  $\pm 45^\circ$  to the longitudinal axis of the snout (i.e., an antisymmetric [ $\pm 45^\circ$ ] angle-ply laminate). We previously identified these modifications to the composite structure of the cuticle within a single species, *Curculio longinasus* Chittenden, 1927 [1, 14]. However, this composite profile is herein reported in the rostrum of six additional, phylogenetically disjoint, species, suggesting that this is an evolutionarily conserved trait throughout the genus *Curculio*. In all examined species, the portion of the snout between the head capsule and apex of the scrobe exhibits a gradual transition in composite profile along an anterior-posterior gradient.

Here we estimate the effect of differential cuticle organization on uni-axial membrane and on transverse flexural Young's moduli of the cuticle in the rostral apex and head capsule using CLPT [32, 33]. The effective elastic constants of the cuticle regions of *Curculio longinasus* – estimated previously [1] – are used to construct constitutive equations for the entire cuticle of that species.

The cuticle of the head capsule is estimated to have membrane and flexural moduli of  $E_m = 4.77 \text{ GPa}$  and  $E_f = 6.04 \text{ GPa}$ , respectively. In the rostral apex these values are reduced by approximately 72% and 60%, respectively ( $E_m = 1.36 \text{ GPa}$ ;  $E_f = 2.44 \text{ GPa}$ ). Two hypothetical cuticle lay-ups are also modeled to individually assess the contributions of either modified layer thickness or stacking angle sequence to the cuticle's flexibility. The effective moduli of a configuration with the angle stacking sequence of an otherwise typical cuticle (i.e., in the head capsule) that shows layer thicknesses of the rostral apex are calculated as  $E_m = 3.73 \text{ GPa}$ ,  $E_f = 4.31 \text{ GPa}$ ; representing 22% and 29% decreases from unmodified cuticle, respectively. Similarly, a hypothetical cuticle with the layer thicknesses of ordinary cuticle yet possessing the angle stacking sequence of the rostral apex (i.e.,  $\pm 45^\circ$  angle-ply in the endocuticle) has effective elastic moduli of  $E_m = 3.77 \text{ GPa}$ ,  $E_f = 5.76 \text{ GPa}$ ; representing 21% and 4.7% decreases from unmodified cuticle, respectively. Each of the cuticle modifications noted in the rostral apex individually decrease the elastic moduli of the cuticle. However, they appear to have a synergistic combined effect on cuticle elasticity, rather than a simple additive effect. This result suggests that both modifications are necessary in order for the snout to function properly in the living individual – where the combined effect allows the rostrum to bend until completely straight without fracture.

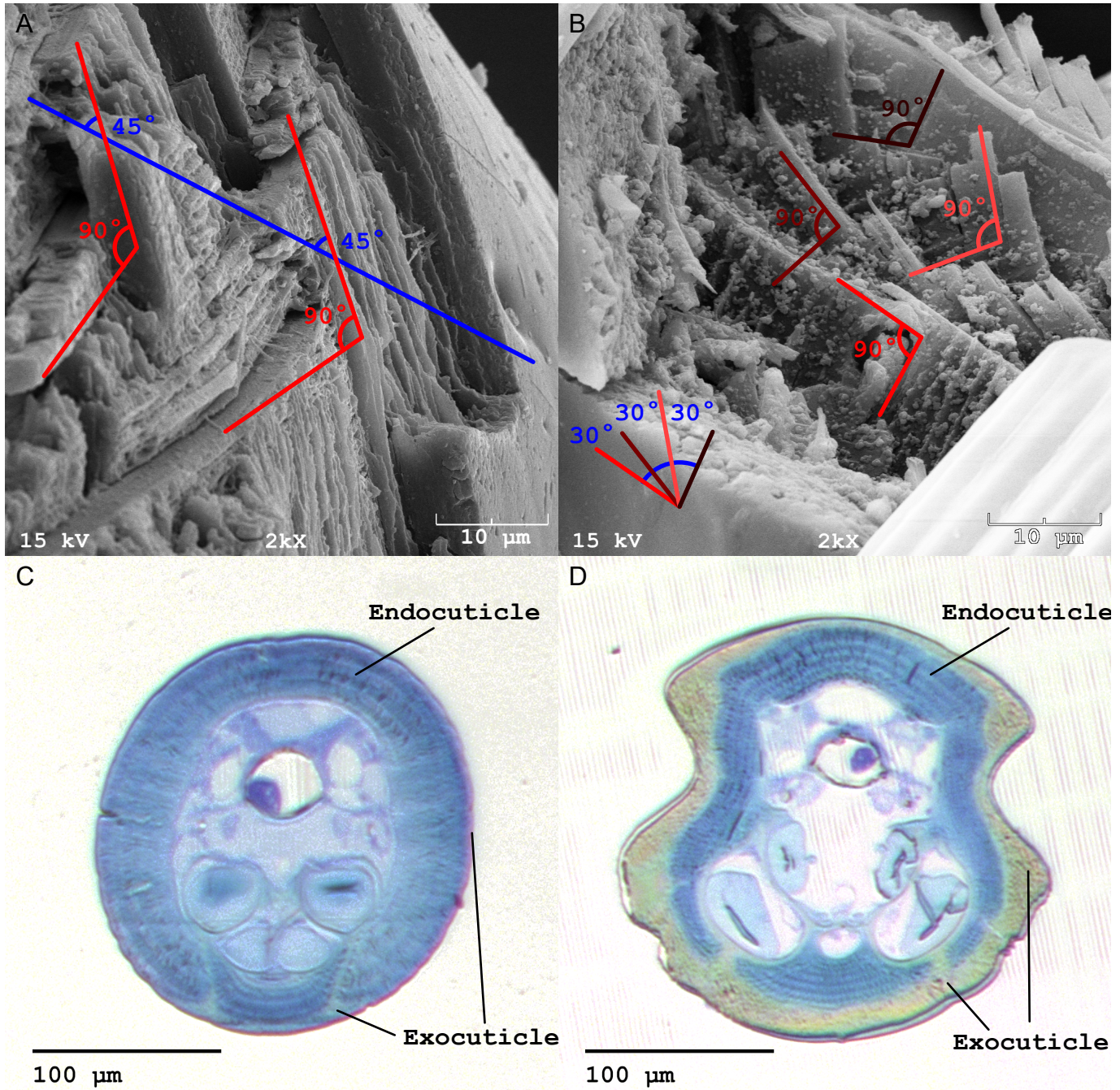


**FIG. 3. Composite profiles of rostral *Curculio* cuticle.** **a**, Scanning electron micrograph of a fractured specimen of *Curculio humeralis* (Casey, 1897), showing that the cuticle of the rostral apex is organized as a  $\pm 45^\circ$  angle-ply laminate. **b**, Scanning electron micrograph of a fractured specimen of *Curculio caryae* (Horn, 1873), showing that the cuticle of the rostral base and head capsule has an approximately  $30^\circ$  stacking angle between each pair of pseudo-orthogonal plies. **c–d**, Semi-thin sections of cuticle from a specimen of *Curculio humeralis*, stained with toluidine-blue-borax; demonstrating: (**c**) that the exocuticle of the rostral apex is reduced to a thin shell close to  $5\ \mu\text{m}$  thick, with the endocuticle thickened to maintain a constant laminate thickness; and, (**d**) that the exocuticle of the head capsule and base of the snout occupies nearly half of the through-thickness of the cuticle.

170      **II. FORCE-CONTROLLED LOADING TO  
171      FRACTURE**

172      To better characterize the failure behavior of the fe-  
173      male rostrum, we performed tensile testing on the snouts  
174      of six *Curculio* species that representing a mixture of  
175      closely and distantly related taxa [34–37]. Each specimen  
176      was first immersed in di-H<sub>2</sub>O for 24 hours to simulate the  
177      living tissue (see [38]), then subjected to force-controlled,  
178      uniaxial loading to fracture at a constant stress rate  
179      of 1.0 gf · s<sup>-1</sup>. In general, the specimens exhibited a  
180      non-linear viscoelastic response curve characterized by  
181      a sharp increase in stress at higher strains, terminating  
182      in brittle fracture [39]. We suggest that strain harden-  
183      ing occurs as the longitudinal axis of the macrofibers be-  
184      comes more closely aligned to the cylindrical axis of the  
185      rostrum, thereby resisting tension more directly with in-  
186      creasing strain [40].

187      We also examined the correspondence between com-  
188      posite structure and mechanical behavior of the snout  
189      in an evolutionary, comparative context. Phylogenetic  
190      linear mixed effects models (PGLM, Fig. 4) were used  
191      to account for phylogenetic non-independence in residual  
192      variance, with species membership included as a random  
193      effect [41, 42]. The resulting models show that the max-  
194      imum force sustained at the site of failure is strongly  
195      correlated with the cross-sectional area of the endocutu-  
196      cle ( $\hat{\beta} = 1.28$ ,  $p < 0.0001$ ), and not the exocuticle ( $\hat{\beta} =$   
197      0.17,  $p = 0.38$ ), at that site. There is thus a negative  
198      correlation between ultimate tensile strength of the spec-  
199      imen and the cross-sectional exocuticle-to-endocuticle  
200      area ratio at the fracture site ( $\hat{\beta} = -0.36$ ,  $p = 0.017$ ).  
201      Although CLPT predicts a positive association between  
202      the proportion of exocuticle and stiffness of a general-  
203      ized cuticle, we found no evidence of correspondence be-  
204      tween the cross-sectional properties of the fracture site  
205      and the overall performance of the rostrum. Because the  
206      cross-sectional areas of the cuticle regions vary across the  
207      length of the head along an anterior-posterior gradient, it  
208      is not possible to correlate measurements from the frac-  
209      ture surface to properties of the entire rostrum. *[NMF*  
210      ***note: How surprising/unexpected is this? If a lot***  
211      ***— state so..]***

212      Instead, we found that the uniaxial elastic modulus  
213      (low strain:  $E_{low}$ ) and secant modulus at failure ( $E_{sec}$ )  
214      were inversely correlated with ultimate strain and frac-  
215      ture toughness (see Fig. 4). This implies that stiffer  
216      specimens – and by extension, stiffer cuticle profiles –  
217      are generally more brittle. We also observed a moder-  
218      ate, but not statistically significant, stiffening size-effect  
219      with respect to rostral length. This runs contrary to  
220      our expectation that a longer, more strongly curved ros-  
221      trum would require increased flexibility to avoid fracture  
222      during oviposition [36, 37]. It is possible that longer ros-  
223      tra also have a longer transition gradient from basal to  
224      apical profile; thereby reinforcing the junction between  
225      the rostrum and head capsule against buckling. Young’s  
226      modulus of the rostrum would be comparatively higher

227      in such species, due to the higher volume fraction of ex-  
228      ocuticle. We therefore posit that the gross elastic per-  
229      formance of the cuticle is consistent across the weevil  
230      genus *Curculio*. A *single* mechanism – i.e., the modi-  
231      fied composite profile – likely confers increased flexibility  
232      and tensile strength to the rostral apex across all *Cur-*  
233      *culio* species. In addition, the endocuticle demonstra-  
234      bly contributes more to rostral tensile strength than the  
235      exocuticle; likely because of its organization into large  
236      bundles of aligned, anisotropic fibers, and amounting a  
237      trade-off between rigidity and toughness. Consequently,  
238      the altered composite profile of the cuticle in the rostral  
239      apex makes the rostrum simultaneously more flexible and  
240      fracture-resistant.

241      **III. LOAD CYCLING OF THE PECAN WEEVIL**

242      To confirm that repeated, prescribed straightening of  
243      the rostrum does not result in damage to the cuticle,  
244      we performed displacement-controlled fatigue testing on  
245      a typical female specimen of the pecan weevil *Curculio*  
246      *caryae* (Horn, 1873) – a species that exhibits extreme  
247      (80–90°, Fig. 5) rostral curvature [16, 21]. The specimen  
248      was aligned so that uniaxial tension would induce elonga-  
249      tion of the distal portion of the rostrum with minimal  
250      off-axis deflection of the uncurved section. The strain  
251      per cycle was fixed at an amplitude sufficient to com-  
252      pletely elongate the rostrum and generate a tensile load of  
253      1.0 N in the straightened configuration (ca. 20% ultimate  
254      strength), at a frequency of 0.33 Hz. The test was termi-  
255      nated after a period of two weeks – i.e., ca. 400,000 cycles  
256      – when the stress amplitude appeared to reach an asym-  
257      totic minimum. The rostrum behaved viscoelastically,  
258      indicated by hysteresis in the stress-strain relationship  
259      during each cycle. Strain amplitude decreased logarith-  
260      mically with cycle number, and the specimen appeared  
261      to have been deformed plastically and permanently dur-  
262      ing the test. However, after cleaning the specimen in a  
263      24-hour wash with ethanol and water, the rostrum had  
264      returned to its original shape (Fig. 5).

265      While we cannot fully determine the cause for ros-  
266      trum stress relaxation *after* testing, we speculate that  
267      it arose from the general mechanism associated with cu-  
268      ticle viscoelasticity. The endocuticle is made of aligned  
269       $\alpha$ -chitin nanofibrils whose crystalline structure is enforced  
270      by hydrogen bonds between individual chitin chains and  
271      through the protein matrix along their length. Macro-  
272      scopic viscoelastic behavior results from slippage between  
273      these chains in response to shearing between the chitin  
274      molecules [2, 43, 44]. Repeated strain may have caused  
275      such slippage in the endocuticle of the rostral apex during  
276      the fatigue test. Without sufficient time for the material  
277      to completely relax after deformation, the rostrum would  
278      slowly accumulate strain and deform viscoelastically [40].  
279      After immersion in ethanol and water, however, the cuti-  
280      cle would be sufficiently plasticized to allow the rostrum  
281      to return to its original configuration, thus dissipating

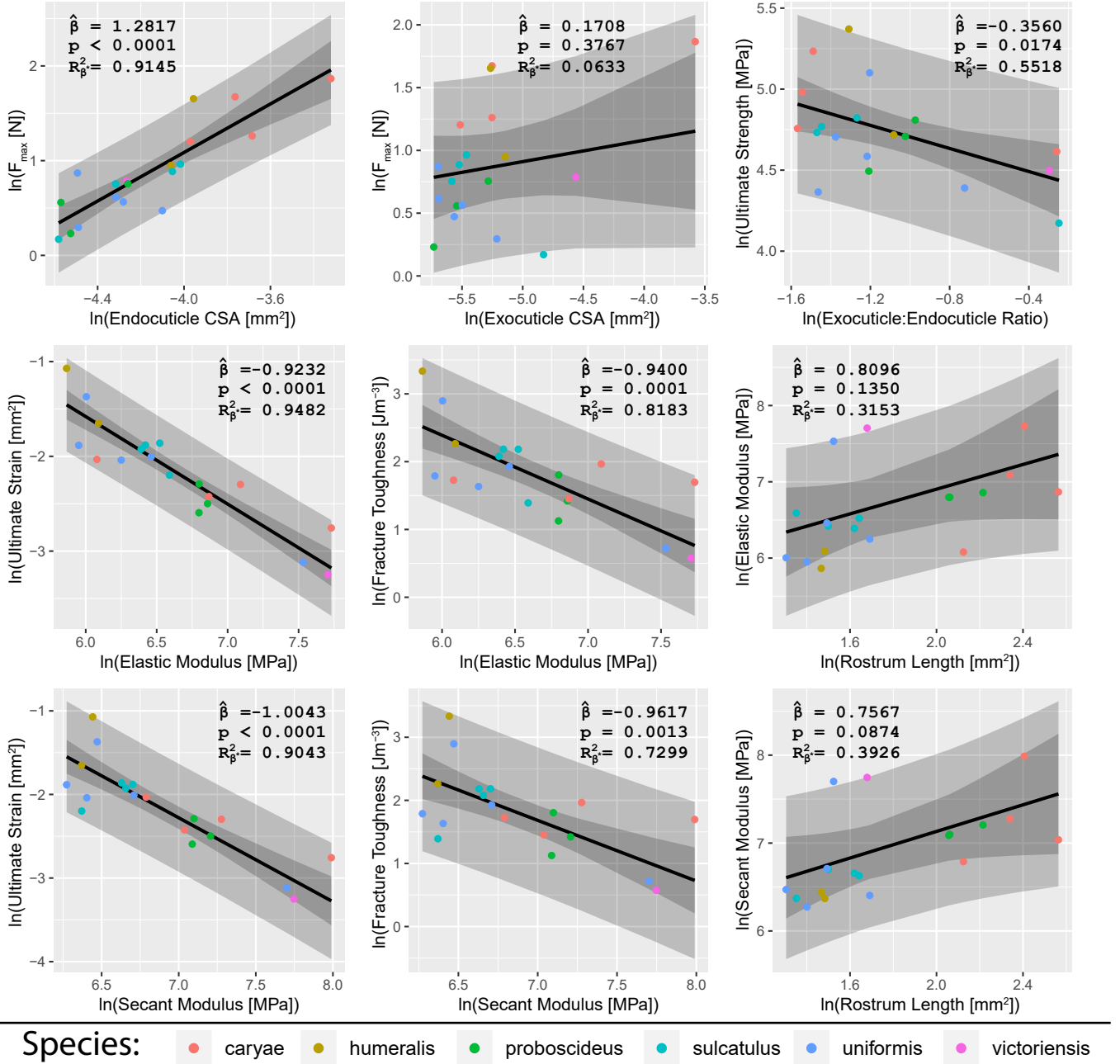


**FIG. 4. Tensile properties of the female *Curculio* rostrum.** Each plot shows the relationship between two variables as predicted by a phylogenetic linear mixed-effect model; with species as a random effect and a variance-covariance matrix generated from Brownian motion over the preferred phylogeny of [35]. Gray regions represent the prediction interval and bootstrapped 95% confidence interval of the model. The estimated fixed effect  $\hat{\beta}$  is given, along with the p-value of a t-test assessing whether  $\hat{\beta}$  is significantly different from zero. A generalized marginal  $R_{\beta}^2$  for assessing fixed effects is also reported. In general, increased endocuticle thickness is associated with greater tensile strength, and stiffness is inversely correlated with toughness.

the accumulated strain.

The specimen did not show any evidence of fractures, micro-tears, or shear cusps anywhere in the surface of the exocuticle. Moreover, the tensile strength of the tested specimen's rostrum was consistent with that of other species members ( $F_{max} = 5.02$  N). Surprisingly,

the specimen remained undamaged by the testing. We therefore conclude that under normal life conditions, repeated bending of the rostrum does not exceed the yield strength of the cuticle.

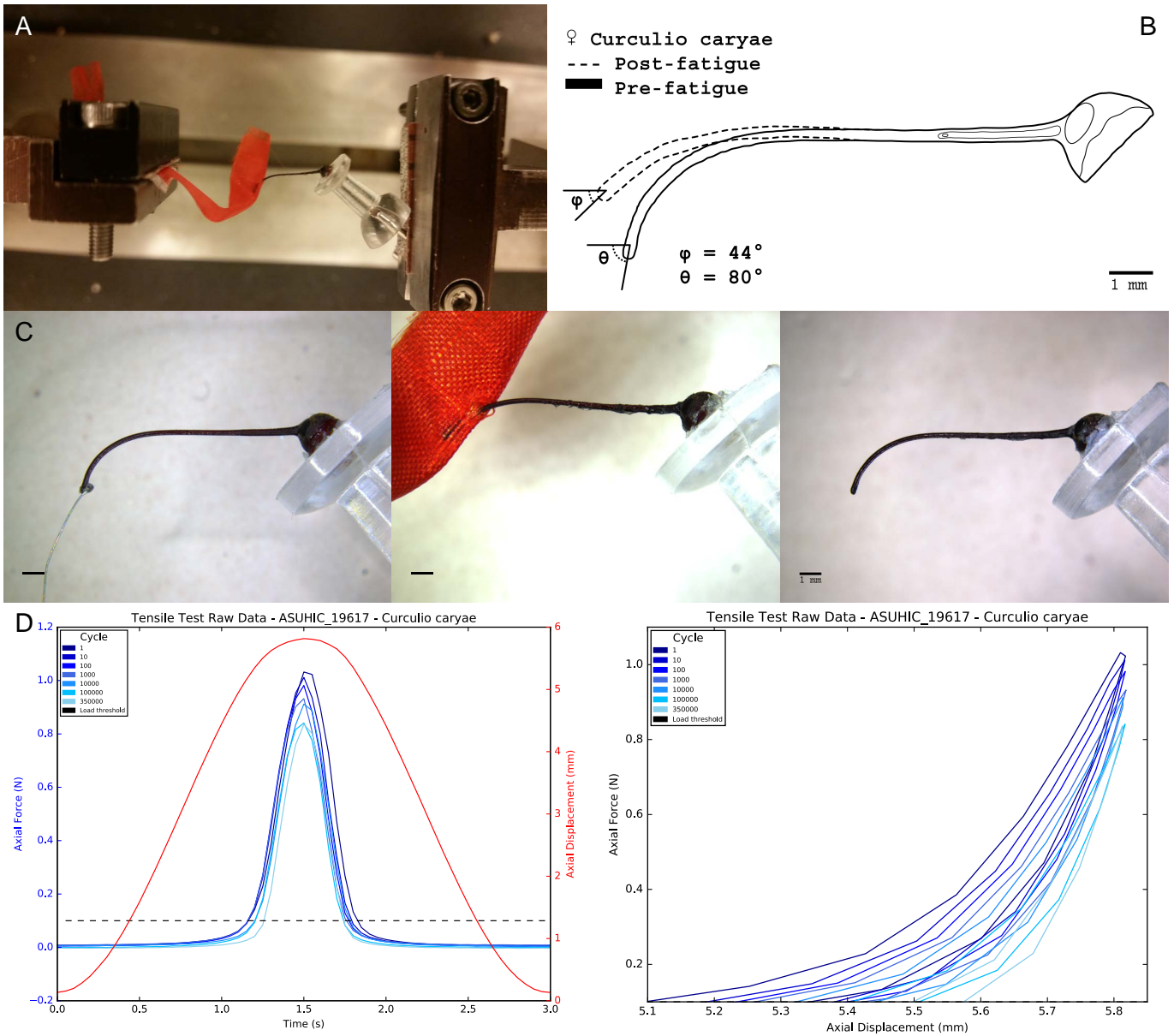


**FIG. 5. Fatigue testing of a female *Curculio caryae* rostrum.** **a**, Set-up of fatigue testing, with the female's head capsule fixed to a pedestal and the rostrum attached to a strip of rip-stop nylon fabric using cyanoacrylate adhesive. The specimen was loaded in tension, as opposed to compression, therefore isolating the effect of tension on the fatigue behavior of the rostrum. **b**, Overlay of the pre- and post-fatigue states of the head, showing a clear (short-term) effect from repeated prescribed strain. **c**, Three-photograph sequence of pre- and post-fatigue states of the rostrum; with the left and central panels showing the conditions immediately prior to and after the testing, respectively, whereas the right panel shows the head having returned to its original shape after 24 hours off soaking in a water/ethanol mixture. Hence the immediate post-fatigue shape is not permanent. **d**, Raw force data (left) and displacement data (right) plots for the fatigue test. The displacement data plot shows clear viscoelastic behavior, indicated by hysteresis in the stress-strain response of the specimen, and exhibits a logarithmic decrease stress amplitude over time.

292     **IV. FRACTOGRAPHY OF CURCULIO TEST  
293     SPECIMENS**

294     In light of the complex failure modes evident in the  
295     fractured specimens, it was not always possible to iden-  
296     tify void nucleation and crack initiation sites. We ob-

297     served several patterns characteristic of both the micro-  
298     scale behavior of the cuticle and the meso-scale behavior  
299     of the rostrum during uniaxial tensile failure (Fig. 6).  
300     These patterns are described below.

301     In transverse view, the exocuticle consistently pre-  
302     sented a nearly continuous fracture surface. This is char-

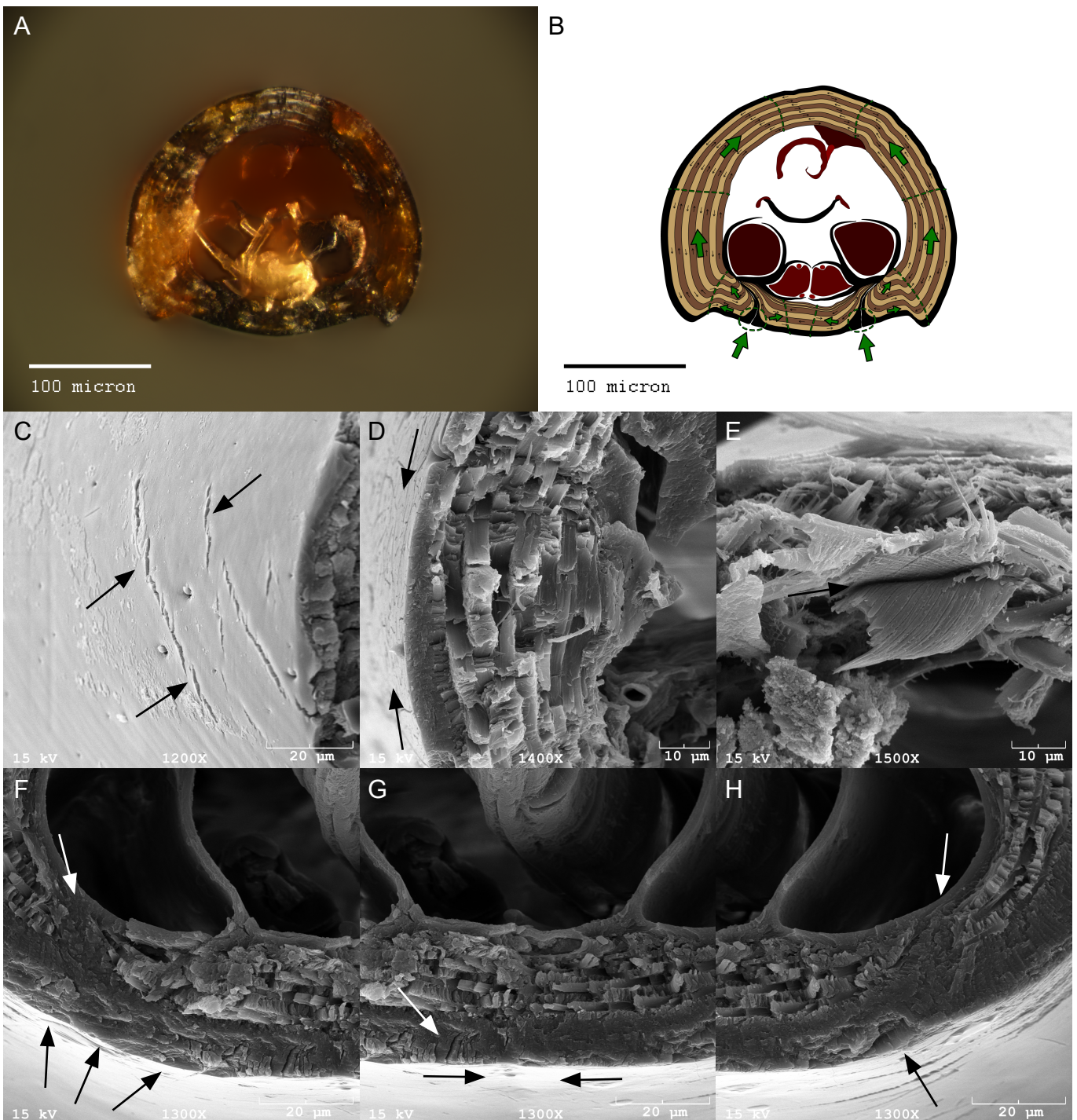


**FIG. 6. Fractography of the female *Curculio* rostrum.** **a**, Light micrograph showing the fracture surface of a tensile tested *Curculio caryae* rostrum, displaying a typical failure mode; illustrated in **(b)**: The small, black arrows indicate the winding direction of the macrofiber lamina; green arrows and dotted lines indicate the direction of crack. Scanning electron micrographs highlight: **(c)** shear cusp formation; **(d)** tensile failure and off-axis macrofiber fiber-pulling; **(e)** interlaminar delamination; **(f-h)** crack formation near invaginated exocuticle; and **(g)** ventral crack-front coalescence and shear cusp formation.

acteristic of comparatively brittle failure – presumably due to the relatively homogeneous arrangement of  $\alpha$ -chitin laminae in the Bouligand structure [25, 26]. The exocuticle typically appeared to fracture at lower strains

than the endocuticle, with shear-cusp formation evident both at the fracture surface and across exocuticle adjacent to the plane of fracture [45]. Conversely, the endocuticle exhibited severe delamination, off-axis ply-splitting,

and fiber-pulling away from the fracture surface. This is indicative of the relatively high toughness of the unidirectional  $\alpha$ -chitin organization within the macrofibers [4, 5]. Because the exocuticle of weevils is anchored to the endocuticle by cross-linking fibers (see [5, 23]), exocuticular shear-cusp formation in uniaxial tension suggests extension-shear coupling within individual endocuticle laminae; and further implies that ply-splitting occurred via mode II fracture between macrofibers at high strain [32, 33]. We hypothesize that intra-laminar extension-shear coupling also yielded off-axis, in-plane resultant forces as a function of lamina orientation angle. Mode III shearing then occurred between laminae with opposing in-plane resultant forces, causing the observed inter-ply delamination. Tensile failure of the macrofiber laminae would ultimately occur via mixed-mode I/II – i.e., transverse tension/intra-laminar shear – fracture, due to an increase in applied stress caused by ply-splitting in adjacent laminae [45].

At the meso-scale, most specimens fractured along a single plane across and between the occipital sulci, which are cuticular invaginations that traverse the entire length of the rostrum [13, 17]. These sulci increase the volume fraction of exocuticle in the ventral part of the snout. They contain large interfaces ideal for void nucleation (Fig. 6). The exocuticle of the occipital sulci usually displayed shear cusps oriented outward from the center of the invagination, and continuing dorsolaterally and ventromedially. Ventrally, the cusps converged toward a prominent scarp where the crack fronts joined. This scarp was often obscured by delaminated endocuticular macrofibers in specimens with large cross-sectional areas of endocuticle,

The first layer of endocuticle usually fractured along the same plane as the exocuticle. Ventrally, the endocuticle laminae typically converged toward a scarp-like region characterized by severe delamination and numerous de-bonded macrofibers. Moreover, macrofibers aligned with the direction of crack propagation exhibited extensive ply-splitting with intermittent transverse shearing. In contrast, macrofibers oriented against the direction of crack propagation primarily displayed fracture by transverse shear along the plane of ply-splitting in adjacent laminae. Because the laminae form a cylinder, contralateral fibers in the same lamina display opposing fracture modes. The ventrolateral surfaces often exhibited extensive inter-ply delamination and fiber de-bonding in scarp-like prominences. This is likely due to a combination of tensile failure and shearing along the dorsally-radiating crack front. Dorsally, the coalescent crack fronts often caused significant de-bonding and ply-splitting, followed by broom-like tensile failure. In some specimens, the contralateral crack fronts were out of plane and coalesced via transverse shear through a large dorsal section of cuticle.

Based on these failure patterns, we hypothesize that the exocuticle-rich occipital sulci are the most likely site for the initiation of void nucleation and catastrophic failure of the integrated rostral cuticle in cross section, as

illustrated in Fig. 6. Structural failure would take place as cracks propagate through the endocuticle from these sutures, and ultimately penetrating the entire thickness of the laminate [13]. Although other, more complex failure modes have been observed, we posit that in live specimens this is the most likely mechanism of tensile failure because typical bending behavior generates tension *only* along the ventral surface of the rostrum.

## V. CONCLUSIONS

The rostrum of *Curculio* is characterized by a discontinuous composite profile. The cuticle is strongly differentiated in terms of relative layer thicknesses and orientation angles along an anterior-posterior gradient. These modifications are sufficient to achieve a marked reduction in the effective membrane and flexural moduli of the cuticle – 72% and 60%, respectively – in constitutive models based on CLPT, thereby accounting for the observed flexibility of the rostral apex in live specimens. However, the reductions can only be realized with *both* modifications to the cuticle, which have a non-additive effect on cuticle elasticity. *Curculio* females require both modifications to function properly during oviposition.

Likewise, tensile and fatigue testing reveal a trade-off between stiffness and fracture resistance – measured by ultimate strain and toughness – mediated by the relative proportion of endocuticle in the laminate. The altered composite profile of the cuticle in the rostral apex makes the rostrum simultaneously more flexible and fracture resistant, permitting the structure to be flexed without exceeding the elastic limits of the cuticle.

This is to our knowledge the first time in arthropods that the composite profile of the cuticle has been related to a gradient in elasticity and tensile performance across a cuticular structure. Because these associations are independent of species membership, we posit that the behavior of the cuticle is consistent across the genus. Rostral flexibility is achieved exclusively in all *Curculio* species through a modified cuticle lay-up. This inference raises the intriguing possibility that a single ancestral shift in cuticle organization at the rostral apex – yielding higher flexibility and tensile strength – enabled the evolutionary “exploration” of a large morphospace region, promoting the high species-level diversity of this lineage.

Based on fractographic analysis of the test specimens, we infer that the exocuticle exhibits brittle fracture at a comparatively low strain, due to shearing between the endocuticle macrofibers to which it is anchored. These macrofibers fail at higher strain, mediated by mixed-mode shearing and tensile fracture within and between laminae. This outcome is consistent with behavior shown in previous studies, as well as theoretical consideration of cuticle microstructure in CLPT. The latter predicts extension shear-coupling ( $A_{16}, A_{26} \neq 0$ ) for individual off-axis macrofiber laminae [32, 33].

Our results imply that fracture initiation occurs in the comparatively brittle exocuticle. The reduction in exocuticle thickness in the rostral apex might serve to mitigate crack formation in rostral bending. Based on this pattern of fracture behavior, we identified the exocuticle-rich occipital suture as a common point of void nucleation and crack initiation. From an evolutionary perspective, these findings reveal an unexpected morphological source of constraint on rostral flexibility, raising the intriguing possibility that this system evolved primarily via negative selection of fracture, rather than positive selection of flexibility. In particular, the cuticle is invaginated in precisely the portion of the snout that experiences the greatest degree of tension during antero-dorsal flexion. The doubly-thick exocuticle in the invagination thus creates an unavoidable, brittle weak-point in an otherwise

endocuticle-dominated rostral apex. This constraint – in conjunction with the minimization of exocuticle thickness in the rostral apex and the increased toughness derived from a thickened endocuticle – lead us to consider that avoidance of catastrophic structural failure has been a driving selective pressure in the evolution of the female *Curculio* rostrum.

## VI. METHODS

Methods, including statements of data availability and any associated accession codes and references, are available in the online version of this paper.

## REFERENCES

- [1] Jansen, M. A., Singh, S. S., Chawla, N., & Franz, N. M. A multilayer micromechanical model of the cuticle of *Curculio longinasus* Chittenden, 1927 (Coleoptera: Curculionidae). *J. Struct. Biol.* **195**: 2, 139–158, (2016).
- [2] Vincent, J. F. V. & Wegst, U. G. K. Design and mechanical properties of insect cuticle. *Arthropod Struct. Dev.* **33**:3, 187–199, (2004).
- [3] Hepburn, H. R. & Ball, A. On the structure and mechanical properties of beetle shells. *J. Mater. Sci.* **8**:5, 618–623, (1973).
- [4] van de Kamp, T. & Greven, H. On the architecture of beetle elytra. *Entomol. Heute* **22**, 191–204, (2010).
- [5] van de Kamp, T., Riedel, A. & Greven, H. Micromorphology of the elytral cuticle of beetles, with an emphasis on weevils (Coleoptera : Curculionoidea) *Arthropod Struct. Dev.* **45**:1, 14–22, (2016).
- [6] Neville, A. C., Parry, D. A. & Woodhead-Galloway, J. The chitin crystallite in arthropod cuticle. *J. Cell Sci.* **21**:1, 73–82, (1976).
- [7] Amini, S., Tadayon, M., Idapalapati, S., and Miserez, A. The role of quasi-plasticity in the extreme contact damage tolerance of the stomatopod dactyl club *Nat. Mater.* **14**:9, 943–950, (2015).
- [8] McCullough, E. L., Tobalske, B. W., and Emlen, D. J. Structural adaptations to diverse fighting styles in sexually selected weapons *Proc. Natl. Acad. Sci. USA* **111**:40, 14484–14488, (2014).
- [9] McCullough, E. L. Mechanical limits to maximum weapon size in a giant rhinoceros beetle *Proc. R. Soc. B* **281**, 20140696, (2014).
- [10] Dirks, J., Parle, E., and Taylor, D. Fatigue of insect cuticle *J. Exp. Biol.* **216**:10, 1924–1927, (2013).
- [11] Dirks, J. and Taylor, D. Fracture toughness of locust cuticle *J. Exp. Biol.* **215**:9, 1502–1508, (2012).
- [12] International Code of Zoological Nomenclature Fourth Edition. (The International Trust for Zoological Nomenclature, London, 1999).
- [13] Davis, S. R. *Morphology, phylogeny, and evolutionary development in the weevils (Insecta: Coleoptera: Curculionoidea)* (Ph.D. thesis, University of Kansas, 2014).
- [14] Singh, S. S., Jansen, M. A., Franz, N. M., and Chawla, N. Microstructure and nanoindentation of the rostrum of *Curculio longinasus* Chittenden, 1927 (Coleoptera: Curculionidae) *Mater. Charact.* **118**, 206–211, (2016).
- [15] Toju, H. and Sota, T. Imbalance of predator and prey armament: geographic clines in phenotypic interface and natural selection *Am. Nat.* **167**:1, 105–117, (2006).
- [16] Gibson, L. P. Monograph of the genus *Curculio* in the New World (Coleoptera: Curculionidae). Part I. United States and Canada *Misc. Publ. Entomol. Soc. Am.* **6**, 239–285, (1969).
- [17] Dennell, R. The structure and function of the mouth-parts, rostrum and fore-gut of the weevil *Calandra granaria* L. *Phil. Trans. R. Soc. Lond. B* **231**:581, 247–291, (1942).
- [18] Morimoto, K. and Kojima, H. Morphologic characters of the weevil head and phylogenetic implications (Coleoptera, Curculionoidea) *Esakia* **43**, 133–169, (2003).
- [19] Ting, P. C. Feeding mechanisms of weevils, their function, and relationship to classification *Mon. Bull. Dep. Agric. State Calif.* **22**, 161–165, (1933).
- [20] Ting, P. C. The mouth parts of the coleopterous group Rhynchophora *Microentomology* **1**, 93–114, (1936).
- [21] Aguirre Uribe, L. A. *Biology of the immature stages of the pecan weevil Curculio caryae (Horn) and oviposition habits of the adult weevil* (Ph.D. thesis, Texas A & M University, 1978).
- [22] Moffett, M. Life in a nutshell *Natl. Geogr. Mag.* **176**, 783–784, (1989).
- [23] Longhai, L. et al. Microstructure and mechanical properties of rostrum in *Cyrtotrachelus longimanus* (Coleoptera: Curculionidae) *Anim. Cells Syst.* **21**:3, 199–206, (2017).
- [24] Matsumura, Y., Kovalev, A. E., and Gorb, S. N. Penetration mechanics of a beetle intromittent organ with bending stiffness gradient and a soft tip, *Sci. Adv.* **3**:12, eaao5469, (2017).
- [25] Nikolov, S. et al. Robustness and optimal use of design principles of arthropod exoskeletons studied by ab initio-based multiscale simulations. *J. Mech. Behav. Biomed. Mater.* **4**:2, 129–145, (2011).

- [26] Nikolov, S. et al. Revealing the design principles of high-performance biological composites using Ab initio and multiscale simulations: The example of lobster cuticle. *Adv. Mater.* **22:4**, 519–526, (2010).
- [27] Blackwell, J. and Weih, M. Structure of chitin-protein complexes: ovipositor of the ichneumon fly *Megarhyssa*. *J. Mol. Biol.* **137:1**, 49–60, (1980).
- [28] Bouligand, Y. Twisted fibrous arrangements in biological materials and cholesteric mesophases. *Tissue Cell* **4:2**, 189–217, (1972).
- [29] Vincent, J. F. V. *Structural biomaterials* (Halsted Press, New York, 1982).
- [30] Cheng, L., Wang, L., & Karlsson, A. M. Mechanics-based analysis of selected features of the exoskeletal microstructure of *Popillia japonica*. *Mater. Res.* **24:11**, 3253–3267, (2009).
- [31] Leopold, R. A., Newman, S. M., and Helgeson, G. A comparison of cuticle deposition during the pre-and post-closion stages of the adult weevil, *Anthonomus grandis* BOHEMAN (Coleoptera: Curculionidae). *Int. J. Insect Morphol. and Embryol.*, **21:1**, 37–62, (1992).
- [32] Reddy, J. N. *Mechanics of laminated composite plates and shells: theory and analysis* (CRC Press, Philadelphia, 2004).
- [33] Jones, R. M. *Mechanics of composite materials* (CRC press, Philadelphia, 2014).
- [34] Hughes, J. and Vogler, A. P. The phylogeny of acorn weevils (genus *Curculio*) from mitochondrial and nuclear DNA sequences: the problem of incomplete data. *Mol. Phylogenet. Evol.* **32:2**, 601–615, (2004).
- [35] Bonal, R. et al. Diversity in insect seed parasite guilds at large geographical scale: the roles of host specificity and spatial distance. *J. Biogeogr.* **43:8**, 1620–1630, (2016).
- [36] Hughes, J. and Vogler, A. P. Ecomorphological adaptation of acorn weevils to their oviposition site. *Evolution* **58:9**, 1971–1983, (2004).
- [37] Bonal, R., Espelta, J. M., and Vogler, A. P. Complex selection on life-history traits and the maintenance of variation in exaggerated rostrum length in acorn weevils. *Oecologia* **167:4**, 1053–1061, (2011).
- [38] Klocke, D. & Schmitz, H. Water as a major modulator of the mechanical properties of insect cuticle. *Acta Biomater.* **7**, 2935–2942 (2011).
- [39] Mihai, L. A. and Goriely, A. How to characterize a non-linear elastic material? A review on nonlinear constitutive parameters in isotropic finite elasticity. *Phil. Trans. R. Soc. Lond. A* **473:2207**, 20170607, (2017).
- [40] Münter, S. et al. Strain history dependence of the nonlinear stress response of fibrin and collagen networks. *Proc. Natl. Acad. Sci. USA* **110:30**, 12197–12202, (2013).
- [41] Felsenstein, J. Phylogenies and the comparative method. *Am. Nat.* **125:1**, 1–15, (1985).
- [42] Revell, L. J. Phylogenetic signal and linear regression on species data. *Methods Ecol. Evol.* **1:4**, 319–329, (2010).
- [43] Beament, J. W. L., Treherne, J. E., and Wigglesworth, V. B. *Advances in insect physiology* Volume 4 (Academic Press Inc., London, 1967).
- [44] Sun, J. Y. et al. Differential constitutive equation of elytra cuticle by nanoindentation. *Adv. Mater. Res.*, **343**, 1133–1139, (2012).
- [45] Greenhalgh, E. *Failure analysis and fractography of polymer composites* (CRC Press, Boca Raton, 2009).

## ACKNOWLEDGMENTS

The authors are grateful to Robert Anderson (CMNC), Lourdes Chamorro (USNM), and Charlie O'Brien (CWOB) for their assistance and provision of *Curculio* specimens used in this study. The authors thank Salvatore Anzaldo, Andrew Johnston, Brian Reilly, Sangmi Lee, and other Arizona State University Hasbrouck Insect Collection (ASUHIC) members for their assistance in procuring, treating, and maintaining specimen loans upon entry into the ASUHIC. The authors would also like to thank David Lowry (ASU CLAS Bioimaging Center) for his training and assistance with resin embedding, scanning electron microscopy, and microtomography; and Salvatore Anzaldo for his assistance with histological staining.

## AUTHOR CONTRIBUTIONS

M.A.J. conducted sectioning and staining, microscopy and imaging, tensile and fatigue testing, statistical analysis, and participated in manuscript preparation. J.W. conducted tensile and fatigue testing and participated in manuscript preparation. N.C. facilitated microscopy, tensile and fatigue testing, and participated in manuscript preparation. N.M.F. facilitated specimen acquisition and imaging and participated in manuscript preparation.

## ADDITIONAL INFORMATION

Supplementary information is available in the online version of the paper. Reprints and permissions information is available online at [www.nature.com/reprints](http://www.nature.com/reprints). Correspondence and requests for materials should be addressed to M.A.J.

## COMPETING FINANCIAL INTERESTS

The authors declare no competing financial interests.

630

## METHODS

631

### Specimen acquisition and taxon sampling

632 Specimens for use in tensile and fatigue testing came  
 633 from the Hasbrouck Insect Collection at Arizona State  
 634 University [ASUHIC]. This set of specimens was supple-  
 635 mented with material housed in the following collections,  
 636 using the codens of Arnett et al. [46]:

637 CMNC: Canadian Museum of Nature Collection, Ottawa,  
 638 Ontario, Canada

639 USNM: National Museum of Natural History, Washington,  
 640 D.C., USA

641 Cold fracture, semi-thin sectioning, and tensile testing  
 642 were conducted on randomly chosen female specimens be-  
 643 longing to six *Curculio* species obtainable through field  
 644 work in the southwestern United States and northwest-  
 645 ern Mexico. Taxon sampling was targeted to represent  
 646 a mixture of disparate radiations and sister taxa with  
 647 a variety of rostral morphotypes in accordance with the  
 648 phylogenetic hypotheses of Hughes et al. [34, 36] and  
 649 Bonal et al. [35]. The six species of *Curculio* used herein  
 650 are (in alphabetical sequence): *Curculio caryae* (Horn,  
 651 1873), *Curculio humeralis* (Casey, 1897), *Curculio pro-*  
*boscideus* Fabricius, 1775, *Curculio sulcatulus* (Casey,  
 653 1897), *Curculio uniformis* (LeConte, 1857), and *Cur-*  
*culio victoriensis* (Chittenden, 1904). Specimens were  
 655 identified to taxonomic (species) concepts using [16] and  
 656 other resources.

657

### Histological sectioning

658 To illustrate the relative proportions of the cuti-  
 659 cle regions in cross-section, serial semi-thin sectioning  
 660 was conducted on exemplary female specimens of *Cur-*  
*culio humeralis* and *Curculio longinasus* Chittenden,  
 662 1927. Live specimens of both species were collected into  
 663 95% ethanol for preservation. A female specimen was  
 664 selected; and the rostrum was separated from the head  
 665 capsule with a fine-edged razor blade. The apical 1/4<sup>th</sup>  
 666 of the rostrum was also removed and then discarded. The  
 667 remaining portion of the rostrum and the head capsule  
 668 were then embedded in EMbed812, as follows.

669 The cuticle was first immersed in acetone for 24 hours,  
 670 and then transferred to a 2:1 mixture of acetone to epoxy  
 671 resin. Samples remained at 21°C for 12 hours on a shaker  
 672 table to prevent hardening. They were then transferred  
 673 into a 1:1 mixture of acetone to resin, followed by a 1:2  
 674 mixture (each for 12 hours and at 21°C on a shaker ta-  
 675 ble), before finally being placed into a silicone mold with  
 676 pure resin. The mold was placed into an oven heated  
 677 to 38°C, and the resin was allowed to cure for 24 hours.  
 678 The resulting blocks were machined to prepare the apical  
 679 surface of each sample for microtomy.

680 A Leica Ultracut R Microtome and diamond knife were  
 681 used to expose a cross-section (transverse plane) of the  
 682 apical and basal portions of the rostrum and to remove  
 683 excess material. Semi-thin sections (0.5 µm thick) were  
 684 kept and stained with toluidine-blue-borax for light mi-  
 685 croscopy and imaging.

### Cold-fracture of specimens

687 Two pinned female specimens of each *Curculio* species  
 688 were selected at random and retained for cold-fracturing  
 689 of the rostrum. The heads of the specimens were re-  
 690 moved and cleaned using a 95% ethanol solution and a  
 691 thin paintbrush. Any muscles protruding from the occip-  
 692 ital foramen were removed with a fine-edged razor blade.  
 693 The antennae were removed directly using forceps to pull  
 694 the scape (basal section of antenna) from the antennal  
 695 insertion. Cleaned specimens were stored at -80°C for  
 696 24 hours, then fractured using forceps over a chilled alu-  
 697 minum block. To fracture each specimen, the head cap-  
 698 sule and rostrum were each gripped firmly in a pair of  
 699 forceps. The forceps were then sharply rotated to frac-  
 700 ture the base of the snout via dorsal flexion. The rostrum  
 701 was fractured a second time, after separation from the  
 702 head capsule, using the same procedure. The segmented  
 703 specimens were then placed into individual glass vials to  
 704 protect the fracture surfaces from contamination prior to  
 705 microscopy.

706

### Tensile and fatigue testing

707 *Force-controlled loading to failure.* Five female spec-  
 708 imens of each *Curculio* species were randomly allocated  
 709 for use in tensile testing. The head of each specimen was  
 710 removed, cleaned, and prepared as described above in the  
 711 cold-fracture protocol. To avoid destroying the delicate,  
 712 brittle specimens when gripping the ends of each head,  
 713 a method was devised to create solid handles that could  
 714 be clamped tightly into grips without risk of damage to  
 715 the cuticle.

716 For each head, four 1 cm<sup>2</sup> strips of gaffer tape were cut;  
 717 these were used as gripping and mounting points for the  
 718 specimen. A strip of tape would be laid flat, with a large  
 719 drop of cyanoacrylate glue placed upon the upturned sur-  
 720 face. The curved portion of the snout was then placed  
 721 into the drop, such that the straight portion of the ro-  
 722 strum was aligned perpendicular to the edge of the strip.  
 723 Hardening of the cyanoacrylate effectively embedded the  
 724 curved portion of the snout in a solid mass, isolating a  
 725 straight section of the snout – from the base to a point  
 726 distad of the apex of the scrobe – for testing. A second  
 727 strip of tape was fixed over this mass with an additional  
 728 layer of cyanoacrylate to provide a dorsal gripping sur-  
 729 face for the mass. A small mark was made to indicate  
 730 the extent of the head inside the mass. This embedding  
 731 procedure was repeated for the head capsule, resulting in

732 a finished specimen with anterior and posterior handles  
733 for testing.

734 Prior to testing, each specimen was placed in de-  
735 ionized water for 24 hours to allow full saturation of the  
736 cuticle, simulating the condition of live tissue [38]. Once  
737 removed for testing, the specimen was gripped using the  
738 cyanoacrylate handles at the marked locations immedi-  
739 ately beyond the anterior margin of the rostrum and the  
740 posterior margin of the head capsule. The exposed sec-  
741 tion of the snout was coated in petroleum jelly using a  
742 cotton swab to prevent loss of moisture and stiffening of  
743 the specimen during the test. Specimens were loaded in  
744 a Tryton 250 Microforce Testing System equipped with  
745 a 5N load cell and mechanical clamp grip. All specimens  
746 were subjected to force-controlled uniaxial tension at a  
747 rate of  $1.0 \text{ gf} \cdot \text{s}^{-1}$  until failure, with a sampling interval  
748 of 0.1 s. Engineering stresses ( $\sigma_0 = F/A_0$ ) and strains  
749 ( $\epsilon_0 = \Delta l/l_0$ ) were reported only for specimens that did  
750 not fracture due to strain accumulation at the interface  
751 between the rostrum and the cyanoacrylate handles.

752 *Displacement-controlled cyclic loading.* To confirm  
753 that repeated, complete extension of a strongly curved  
754 rostrum would not result in fracture of the cuticle, a rep-  
755 resentative female specimen of *Curculio caryae* was allo-  
756 cated for fatigue testing. The head capsule of the spec-  
757 imen was fixed to a push-pin using cyanoacrylate glue.  
758 This served as a pedestal and gripping location for the  
759 posterior portion of the specimen. The apex of the ros-  
760 trum was fixed to a strip of ripstop nylon fabric equal  
761 in length to the head, using cyanoacrylate glue. As with  
762 tensile testing, the specimen was placed in de-ionized wa-  
763 ter for 24 hours, then coated in petroleum jelly using a  
764 cotton swab immediately prior to load cycling.

765 The end of the fabric was gripped and used to elon-  
766 gate the rostrum in tension by pulling on the fabric, thus  
767 isolating the effect of tension on the fatigue life of the ros-  
768 tral cuticle. In this way, the rostrum would return to its  
769 original configuration in a spring-like manner, as in liv-  
770 ing specimens, rather than being forced to return to the  
771 initial position. The rostrum was aligned such that com-  
772 plete elongation of the curved section would take place in  
773 tension, with minimal off-axis deflection of the un-curved  
774 section. The specimen was subjected to displacement-  
775 controlled loading sufficient to fully extend the rostrum  
776 and generate a load stress of 1 N, or approximately 20%  
777 of the tensile strength of the species average. Load cy-  
778 cling took place at a rate of 0.33Hz, and was continued  
779 for 14 days – i.e., 400,000 cycles – until the tensile stress  
780 in the sample approached an asymptotic minimum.

781 Once the test was concluded, the specimen was placed  
782 in a 50% ethanol solution for 24 hours to clean the  
783 petroleum jelly from the rostrum. The specimen was  
784 examined for surface fractures and micro-tears, then sub-  
785 jected to tensile testing via the same protocol as the other  
786 specimens to assess whether the cuticle had begun to fa-  
787 tigue.

## Specimen imaging and microscopy

789 The fracture surfaces of cold-fractured specimens were  
790 examined using scanning electron microscopy to charac-  
791 terize the composite profile and microstructure of the  
792 rostrum. Fracture behavior of tensile testing specimens  
793 was assessed using both light microscopy and SEM to  
794 image the fracture surfaces of the specimens in trans-  
795 verse view. Electron microscopy was conducted using  
796 a JEOL JSM6300 scanning electron microscope. Light  
797 microscopy was conducted using a Leica M205 C stere-  
798 omicroscope and attached computer running the software  
799 Leica Application Suite (LAS); as well as a Visionary  
800 Digital Passport II system using a Canon EOS Mark 5D  
801 II camera outfitted with interchangeable macro lenses.  
802 Specimen length, layer thicknesses, macrofiber orienta-  
803 tion angles, and cross-sectional areas were measured in  
804 the LAS and in Adobe Illustrator, using pixel-wise mea-  
805 surements multiplied by a scaling factor for the image.

## Constitutive modeling of the cuticle

807 *General approach.* The effective uni-axial membrane  
808 and transverse flexural elastic moduli of idealized cuti-  
809 cle organizations, representing both the rostral apex and  
810 head capsule, were estimated using Classical Laminate  
811 Plate Theory (CLPT). For general information on this  
812 approach see [32, 33]. The composite profiles of both  
813 types of cuticle were idealized using the layer thicknesses  
814 and stacking sequences observed in *Curculio longinasus*.  
815 This particular species was chosen because we derived  
816 the effective elastic constants of the individual compo-  
817 nents of the cuticle in previous work [1, 14]. In addition,  
818 *Curculio longinasus* exhibits a profile that is typical and  
819 representative for the genus *Curculio*, based on examina-  
820 tion of the six species used for tensile testing.

821 For *Curculio longinasus* the total thickness of the  
822 cuticle in the head and rostrum is roughly 50  $\mu\text{m}$ ,  
823 as in most specimens of the other examined species.  
824 In the head capsule, the exocuticle occupies between  
825 30-50% of the through-thickness of the laminate, with  
826 the remaining thickness nearly evenly divided between  
827 12 layers of endocuticle. We use the maximum (50% of  
828 through-thickness, or 25  $\mu\text{m}$ ) for the model, since the  
829 cuticle appears to deviate from this value only in regions  
830 with sulci (grooves), pores, and other scattered features  
831 of the surface sculpture. The macrofiber laminae of  
832 the endocuticle were assigned a stacking sequence of  
833  $0^\circ, 90^\circ, 30^\circ, -60^\circ, 60^\circ, -30^\circ, 90^\circ, 0^\circ, -60^\circ, 30^\circ, -30^\circ, 60^\circ$ ;  
834 thereby representing pairs of orthogonal plies stacked at  
835 a constant rotation angle of  $30^\circ$ , in approximation of the  
836 living tissue.

837 In the rostral apex, the exocuticle is reduced to a thin  
838 shell approximately 5  $\mu\text{m}$  in thickness, or 10% of the total  
839 cuticle thickness. The endocuticle displays a more com-  
840 plex pattern of layer thicknesses in the rostral apex than  
841 in the head capsule. Each of the eight outermost layers

842 are of nearly equal thickness to the exocuticle (5  $\mu\text{m}$ ),  
 843 whereas the four innermost layers have a combined thick-  
 844 ness equal to that of the exocuticle or to a single layer  
 845 of outer endocuticle ( $h_{\text{outer}} = 5 \mu\text{m}$ ,  $h_{\text{inner}} = 1.25 \mu\text{m}$ ).  
 846 The stacking sequence with respect to the longitudinal  
 847 axis of the rostrum forms an antisymmetric angle-ply  
 848 laminate of  $\pm 45^\circ$ .

849 To assess the individual contributions of layer thickness  
 850 and stacking angle sequence to cuticle flexibility in the  
 851 rostral apex, two hypothetical cuticle lay-ups were mod-  
 852 elled – each with only one of the modifications present in  
 853 the cuticle of the rostral apex. The first of these models  
 854 has the layer thicknesses of the rostral apex, but fiber  
 855 orientations of the head capsule; whereas the second has  
 856 the fiber orientations of the rostral apex, but the layer  
 857 thicknesses of the head capsule.

858 Because these laminates are not symmetric, each has  
 859 a bending-extension coupling matrix  $[B]$  populated with  
 860 non-zero terms; thus complicating the calculation of ef-  
 861 fective in-plane elastic moduli. To circumvent this diffi-  
 862 culty and enable meaningful comparisons between each  
 863 laminate, all of the lay-ups are reflected about their  
 864 inner surface. This effectively doubles their thickness  
 865 while producing a balanced, symmetric laminate with  
 866 no coupling between bending and extension (i.e.,  $[B] =$   
 867  $0_{3,3}$ ). Estimation of in-plane elastic constants from the  
 868 extension( $[A]$ ) and bending ( $[D]$ ) matrices is described  
 869 in detail below. The program Matlab R2018b was used  
 870 to numerically evaluate the final values of the effective  
 871 elastic constants [47].

872 *Classical Laminate Plate Theory.* We begin by calcu-  
 873 lating the 2D reduced stiffness matrix for each part of the  
 874 cuticle. For orthotropic materials with the principal axes  
 875 parallel to the ply edges, the reduced stiffness matrix is  
 876 defined as follows:

$$[Q] = \begin{bmatrix} Q_{11} & Q_{12} & 0 \\ Q_{21} & Q_{22} & 0 \\ 0 & 0 & Q_{66} \end{bmatrix}, \quad (1)$$

877 where:

$$\begin{aligned} Q_{11} &= \frac{E_1}{1 - \nu_{12}\nu_{21}}, \\ Q_{12} &= \frac{E_1\nu_{21}}{1 - \nu_{12}\nu_{21}} = Q_{21}, \\ Q_{21} &= \frac{E_2\nu_{12}}{1 - \nu_{12}\nu_{21}} = Q_{12}, \\ Q_{22} &= \frac{E_2}{1 - \nu_{12}\nu_{21}}, \\ Q_{66} &= G_{12}. \end{aligned} \quad (2)$$

878 For each layer  $k$ , the reduced stiffness matrix is trans-  
 879 formed to account for the layer orientation angle  $\theta$  within  
 880 the laminate coordinate system, yielding a reduced trans-  
 881 formed stiffness matrix according to:

$$[\bar{Q}] = [T]^{-1}[Q][T]^{-T}, \quad (3)$$

882 where the transformation matrix  $[T]$  is defined as:

$$[T] = \begin{bmatrix} \cos^2 \theta & \sin^2 \theta & 2 \cos \theta \sin \theta \\ \sin^2 \theta & \cos^2 \theta & -2 \cos \theta \sin \theta \\ -\cos \theta \sin \theta & \cos \theta \sin \theta & \cos^2 \theta - \sin^2 \theta \end{bmatrix}. \quad (4)$$

883 Using the lay-ups specified for each type of cuticle  
 884 described above, we calculate the extensional stiffness  
 885 matrix  $[A]$ , bending stiffness matrix  $[D]$ , and bending-  
 886 extension coupling matrix  $[B]$  for each laminate consist-  
 887 ing of  $n$  layers at a distance  $z$  from the laminate mid-  
 888 plane. The elements of these matrices can be identified  
 889 according to:

$$\begin{aligned} A_{ij} &= \sum_{k=1}^n (\bar{Q}_{ij})_k (z_k - z_{k-1}), \\ B_{ij} &= \frac{1}{2} \sum_{k=1}^n (\bar{Q}_{ij})_k (z_k^2 - z_{k-1}^2), \\ D_{ij} &= \frac{1}{3} \sum_{k=1}^n (\bar{Q}_{ij})_k (z_k^3 - z_{k-1}^3). \end{aligned} \quad (5)$$

890 These stiffness matrices respectively relate vectors of  
 891 resultant forces  $\{N\}$  and bending moments  $\{M\}$  to mid-  
 892 surface strains and curvatures  $\{\epsilon^\circ\}$  and  $\{\kappa\}$  in the lami-  
 893 nate, according to the following relationship:

$$\begin{Bmatrix} \{N\} \\ \{M\} \end{Bmatrix} = \begin{bmatrix} [A] & [B] \\ [B] & [D] \end{bmatrix} \begin{Bmatrix} \{\epsilon^\circ\} \\ \{\kappa\} \end{Bmatrix}. \quad (6)$$

894 For symmetric laminates,  $[B] = 0_{3,3}$ , and therefore:

$$\begin{aligned} \{N\} &= [A]\{\epsilon^\circ\}, \\ \{M\} &= [D]\{\kappa\}, \end{aligned} \quad (7)$$

895 or, in expanded form:

$$\begin{aligned} \begin{Bmatrix} N_{xx} \\ N_{yy} \\ N_{xy} \end{Bmatrix} &= \begin{bmatrix} A_{11} & A_{12} & A_{16} \\ A_{21} & A_{22} & A_{26} \\ A_{61} & A_{62} & A_{66} \end{bmatrix} \begin{Bmatrix} \epsilon_{xx}^\circ \\ \epsilon_{yy}^\circ \\ \gamma_{xy} \end{Bmatrix}, \\ \begin{Bmatrix} M_{xx} \\ M_{yy} \\ M_{xy} \end{Bmatrix} &= \begin{bmatrix} D_{11} & D_{12} & D_{16} \\ D_{21} & D_{22} & D_{26} \\ D_{61} & D_{62} & D_{66} \end{bmatrix} \begin{Bmatrix} \kappa_{xx} \\ \kappa_{yy} \\ \kappa_{xy} \end{Bmatrix}. \end{aligned} \quad (8)$$

896 If we make the simplifying assumptions [32, 33] that  
 897 (1) the laminate experiences pure axial loading and  
 898 transverse bending (i.e.,  $N_{yy} = N_{xy} = 0$  and  $M_{yy} =$   
 899  $M_{xy} = 0$ , respectively), and (2) the laminate is a beam  
 900 of sufficiently high aspect ratio to minimize the Poisson

effect and anisotropic shear coupling (i.e., below we effectively let  $A_{12}^* = A_{16}^* = 0$  and  $D_{12}^* = D_{16}^* = 0$ ), then we can calculate the in-plane effective flexural and axial Young's moduli of the laminate along the x-axis.

For axial Young's modulus of the laminate, we first define the average membrane stresses in the laminate as:

$$\{\bar{\sigma}^m\} = \frac{\{N\}}{z_1 - z_n}. \quad (9)$$

By substitution in Eq. 7, we obtain:

$$\begin{Bmatrix} \bar{\sigma}_{xx}^m \\ \bar{\sigma}_{yy}^m \\ \bar{\tau}_{xy}^m \end{Bmatrix} = \frac{1}{(z_1 - z_n)} \begin{Bmatrix} A_{11} & A_{12} & A_{16} \\ A_{21} & A_{22} & A_{26} \\ A_{61} & A_{62} & A_{66} \end{Bmatrix} \begin{Bmatrix} \epsilon_{xx}^m \\ \epsilon_{yy}^m \\ \gamma_{xy}^m \end{Bmatrix}, \quad (10)$$

and, by inverting this equation (let  $A^* = A^{-1}$ ) and substituting  $A_{12}^* = A_{16}^* = 0$  based on the assumptions above, we infer:

$$\epsilon_{xx}^m = (z_1 - z_n) A_{11}^* \bar{\sigma}_{xx}^m. \quad (11)$$

We therefore define Young's modulus for effective axial elasticity as:

$$E_{xx}^m = \frac{\bar{\sigma}_{xx}^m}{\epsilon_{xx}^m} = \frac{1}{(z_1 - z_k) A_{11}^*}. \quad (12)$$

To find the transverse flexural Young's modulus of the laminate, we first specify the moment-curvature relation of an Euler-Bernoulli beam:

$$M = EI\kappa. \quad (13)$$

Along the x-axis, the second moment of area for a rectangular cross-section is:

$$I_{yy} = \frac{b(z_1 - z_n)^3}{12}. \quad (14)$$

Given the assumption that  $M_{yy} = M_{xy} = 0$ , the moment along the x-axis is related to the moment of the beam by:

$$M = M_{xx} b. \quad (15)$$

Thus, given the assumption that  $D_{12}^* = D_{16}^* = 0$ , the Young's modulus for the effective transverse flexural elasticity of the laminate can be found by making Eq. 13 specific to transverse flexure of the x-axis and rearranging the terms:

$$E_{xx}^f = \frac{12M_{xx}}{(z_1 - z_n)^3 \kappa_{xx}}. \quad (16)$$

From inversion of Eq. 7 (let  $D^* = D^{-1}$ ), this reduces to:

$$E_{xx}^f = \frac{12}{(z_1 - z_n)^3 D_{11}^*}. \quad (17)$$

## Statistical analysis

*Model selection and fitting.* In order to explore the relationships between the composite structure and mechanical properties of the cuticle, we fit phylogenetic linear mixed-effects models (PGLMM) to the tensile testing data using maximum likelihood estimation [48–51]. Raw data was processed using a custom script in Python version 3.5.2 [52]. Model exploration and fitting was conducted in R version 3.5.1 (2018-07-02) -- ‘Feather Spray’, using the ‘nlme’ and ‘ape’ packages [53–55]. Response variables and covariates were natural-log transformed, as needed, to ensure that the normalized model residuals were normally distributed [R:shapiro.test] and homoscedastic [R:levene.test], using numerical and graphical analysis (see Supplementary Data). In order to control for phylogenetic non-independence in the data, we included the species of each specimen as a random effect in all models. We also allowed for correlation in the error term of the models, as specified by a variance-covariance matrix generated from a Brownian motion model of trait evolution [R:‘ape’:corBrownian] along a phylogeny [54, 56].

The preferred phylogeny for select North American *Curculio* species is that of Bonal et al. [35]. This phylogeny was generated using Maximum-Likelihood methods; it is untrammatic yet has uniform internal branch lengths. The preferred tree was pruned to include only those species used in tensile testing, with a polytomy at each species' root node to represent the individual specimens examined for that species. Because the branch lengths of the tree were not specified, all branch lengths were set equal to 1.

In general, phylogenetic regression is very robust with respect to missing or incomplete branch length data. Underestimation of branch lengths causes overestimation of phylogenetic signal. This phenomenon was not found to be statistically significant for any of our models. Therefore we consider our study's principal findings to be unaffected by branch length underestimation [56–58].

Other models of trait evolution were considered during model exploration; including Ornstein-Uhlenbeck [R:‘ape’:corMartins] and variable rate (AC/DC) [R:‘ape’:corBlomberg] models [54, 56]. However, neither of these produced a significantly better fit to the data than the Brownian motion model for any comparison, as measured by likelihood score and residual variance; viz.  $R_\sigma^2$  and  $R_{\beta^*}^2$  [R:‘r2glmm’:r2beta] (see Supplementary Data).  $R_\sigma^2$  is the proportion of generalized variance explained by fixed effects. This measure is generally used for comparison of covariance structures [59–61].  $R_{\beta^*}^2$  measures the multivariate association between the outcome and the fixed effects within a given correlation structure, and is generally used to compare fixed effects [59–61]. Using the R package ‘phytools’ [56, 62], we also estimated the phylogenetic signal in the residual variance of each model; taking into account two measures of spatial autocorrelation (Abouheif's  $C$  and Moran's  $I$ ),

and two measures of phylogenetic signal (Pagel's  $\lambda$  and Blomberg's  $\kappa$ ).  
section as a fixed effect, with ultimate tensile strength as  
the response variable.

In all models, we tested whether the inclusion of phylogenetic correlation in the model error produced significantly better model fit, using a likelihood-ratio test [R: 'lmtest':lrtest] and  $R^2$ -difference test [R: 'r2glmm':r2beta(method='sgv')] between the fully-specified model and a model lacking the phylogenetic effect [61, 63]. Models that incorporated covariance due to Brownian motion consistently produced higher likelihood scores and fit to the data. However, no model exhibited statistically significant phylogenetic signal in any of the variables. Once models were fitted to the data, T- and F-statistics were calculated to determine whether each cofactor was significantly different from zero.

*Hypothesis testing.* Our objectives for hypothesis testing using the PGLMMs were threefold: (1) to assess whether the altered ratio of exocuticle to endocuticle in the rostral apex has an effect on the tensile strength of the rostrum; (2) to test whether a trade-off exists between specimen stiffness and resistance to fracture; and (3) to examine whether rostrum length and flexibility are correlated.

To test the relationship between relative layer thicknesses and tensile strength, we fitted a fully-specified model with the cross-sectional area of exocuticle and endocuticle at the site of fracture as fixed effects, including an interaction term, and with the maximum tensile force sustained prior to fracture as a response variable. This model was then compared to models with only cross-sectional area of either endocuticle or exocuticle, but not both, as the sole fixed effect in the model. We then tested whether one or both regions were significantly correlated to the maximum force sustained in tension, using likelihood-ratio tests and  $R^2_{\beta^*}$ -difference tests between each of the three models. Only the cross-sectional area of endocuticle produced a significant fixed effect. We therefore elected to make the model more parsimonious by removing cross-sectional area of exocuticle as a fixed effect. The final model generated for our first aim featured the ratio of exocuticle to endocuticle in cross-

For our second aim we examined the relationship between specimen stiffness and resistance to fracture. Specimen stiffness was characterized using a low strain elastic modulus – averaged across the first 33% of the stress-strain curve – and the secant modulus at failure. Resistance to fracture was quantified in terms of ultimate strain and fracture toughness, measured as area under the stress-strain curve. Four models were fitted, two of which had ultimate strain as the response variable, and two with fracture toughness as response variable. Each model then used one of the different measures of specimen stiffness as a fixed effect.

Finally, for the third aim we explored whether a size-effect might exist in the *Curculio* rostrum; and specifically if longer and typically more curved rostra were more flexible than shorter, straighter rostra. We generated two models; the low strain and secant elastic moduli usually served as response variables, with specimen length as the fixed effect in both.

#### Code availability

R, Python, and Matlab scripts used to manipulate and analyze the raw data (as well as their outputs), produce figures, and estimate effective elastic constants are available from the corresponding author upon request.

#### Data availability

Stress-strain curves for all tensile and fatigue-tested specimens are provided as PDFs (Supplement 1). Diagnostic plots for all PGLMMs are provided as PDFs (Supplement 2). PGLMM terms and output are provided in a PDF (Supplement 3). Raw and processed data will be provided by the corresponding author upon reasonable request.

#### REFERENCES

- [46] Arnett Jr., R. H., Samuelson, G. A., and Nishida G. M. *The Insect and Spider Collections of the World, 2nd Edition*. Fauna and Flora Handbook No. 11. (Sandhill Crane Press, Gainesville, 1993).
- [47] The MathWorks, Inc., *MATLAB and Statistics Toolbox* (Natick, Mass., Release R2018b, 2018).
- [48] Galecki, A. and Burzykowski, T. *Linear Mixed-Effects Models Using R. A Step-by-Step Approach* (Springer, New York, 2013).
- [49] Hadfield, J. D. and Nakagawa, S. General quantitative genetic methods for comparative biology: phylogenies, taxonomies and multi-trait models for continuous and categorical characters *J. Evol. Biol.* **23:3**, 494–508, (2010).
- [50] Housworth, E. A., Martins, E. P., and Lynch, M. The Phylogenetic Mixed Model *Am. Nat.* **163:1**, 84–96, (2004).
- [51] Stone, G. N., Sean, N., and Felsenstein, J. Controlling for non-independence in comparative analysis of patterns across populations within species *Philos. Trans. Royal Soc. B* **366:1569**, 1410–1424, (2011).
- [52] Python Core Team. *Python: A dynamic, open source programming language* (Python Software Foundation, Version 3.5.2, 2018).
- [53] R Development Core Team *R: A Language and Environment for Statistical Computing* (R Foundation for Statistical Computing, Vienna, Version 3.5.1, 2008).

- 1088 [54] Paradis, E. and Schliep, K. ape 5.0: an environment  
1089 for modern phylogenetics and evolutionary analyses in  
1090 R *Bioinformatics* **5.0**, (2018).
- 1091 [55] Pinheiro, J. et al. nlme: Linear and Nonlinear Mixed  
1092 Effects Models **R package version 3.1-137**, (2018).
- 1093 [56] Münkemüller, T. et al. How to measure and test phylo-  
1094 genetic signal *Methods Ecol. Evol.* **3:4**, 743–756, (2012).
- 1095 [57] Stone, E. A. Why the phylogenetic regression appears  
1096 robust to tree misspecification *Syst. Biol.* **60:3**, 245–260,  
1097 (2011).
- 1098 [58] Molina-Venegas, R. and Rodríguez, M. Á. Revisiting  
1099 phylogenetic signal; strong or negligible impacts of poly-  
1100 tomies and branch length information? *BMC Evol. Biol.*  
1101 **17:1**, 1–53, (2017).
- 1102 [59] Nakagawa, S. and Schielzeth, H. A general and simple  
1103 method for obtaining R2 from generalized linear mixed-  
1104 effects models *Methods Ecol. Evol.* **4:2**, 133–142, (2013).
- 1105 [60] Jaeger, B. C., Edwards, L. J., Das, K., and Sen, P. K.  
1106 An R<sup>2</sup> statistic for fixed effects in the generalized linear  
1107 mixed model *J. Appl. Stat.* **44:6**, 1086–1105, (2016).
- 1108 [61] Jaeger, B. Computes R Squared for Mixed (Multilevel)  
1109 Models **Version 0.1.2** (2017).
- 1110 [62] Liam, J. R. phytools: An R package for phylogenetic  
1111 comparative biology (and other things) *Methods Ecol.  
and Evol.* **3**, 217–223, (2012).
- 1112 [63] Zeileis, A. and Hothorn, T. Diagnostic Checking in Re-  
1113 gression Relationships *R News* **2:3**, 7–10, (2002).
- 1114